EXHAUSTIVE THEORETICAL INVESTIGATION OF PHONON NUMBER ALTERATION, FUSION CROSS SECTIONS AND BARRIER DISTRIBUTIONS FOR ^{30}Si + ^{90,92,94,96}Zr REACTIONS VIA ENERGY-DEPENDENT WOODS–SAXON POTENTIAL AND COUPLED CHANNEL MODELS

Z.M. Cinan[a], B. Erol[b], T. Baskan[a], A.H. Yilmaz[a]

[a]Department of Physics, Karadeniz Technical University, 61080 Trabzon, Turkey
[b]Department of Physics, Recep Tayyip Erdogan University, 53100 Rize, Turkey

Received 23 July 2021, accepted 30 March 2022, published online 12 April 2022

The fusion cross sections and barrier distributions of stable Zr isotope targets ^{90,92,94,96}Zr with ^{30}Si projectile nuclei are investigated theoretically via the Energy-dependent Woods–Saxon Potential (EDWSP) and Coupled Channel (CC) models. In our calculations, we have taken the bombarding energy range of the projectile–target interaction to be around the Coulomb barrier for all reactions. All theoretical accounts have been worked via the NRV Knowledge Base, the CCFULL code, and Wong's formula. We detailed interrogated the repercussions of phonon number in projectile and target nuclei on heavy-ion fusion cross sections and barrier distributions. Over this investigation, we presented that the EDWSP and CC models, and all computation bases operated to elucidate the fusion cross-section data and barrier distributions are decent. Our theoretical investigation proves the importance of inspecting heavy-ion fusion reactions with theory-based research and encourages new experimental investigations that are not yet included in the literature.

DOI:10.5506/APhysPolB.53.3-A4

1. Introduction

The fusion mechanisms of heavy-ion interactions are very substantial for experimental and theoretical research as they describe the relationship between nuclear structure and reaction technics exhaustively [1–4]. Theoretically, these reactions around the Coulomb barrier region can be contemplated as an extraordinary barrier diffusion issue. The multi-dimensional barrier diffusion situation might be elucidated by sorting out the couple channel equations, namely the Coupled Channel (CC) model [5–7]. Nonetheless, due to the reaction systematics, it is essential to pay attention to an

extensive quantity of channels that are arduous to accomplish in the computation design. Besides, data statistics of the interacting nuclei are also needed as an entrance. Consequently, the CC computations are challenging in manifold computation circumstances.

Various calculation models have been counseled for the parameters of the barrier distributions about the stationary and dynamic deformations of the two interacting nuclei, for the interaction potential among the projectile and the target. For the vibrational and rotational coupling impact, the coefficients of the used models *seriatim* are presented. For the spherical reaction mechanism (vibrational coupled effect), the width of the barrier distribution moves up with the charge yield of the reaction framework, while for the deformed reaction mechanisms (rotational coupled effect), as well as the charge product of the reaction mechanism, the width of the barrier distributions is also concerning the static deformation parameters of the projectile and the target [8]. Generally, the CC model for the coefficients of the barrier distribution operates eminently fine in identifying cross sections and can supply advantageous information concerning cross-section predictions [9–12]. According to many calculation models for fusion reactions, the projectile and target nuclei have to exceed the Coulomb barrier between them, because only then they can form the compound nucleus.

When looking at the studies in the literature, it has been viewed that studies have been taken based on various theoretical approaches *e.g.* combining nuclear structure degrees of freedom such as surface excitations, static deformation, and high degree deformation, and the rotation and/or vibrations of nuclear interacting nuclei to reproduce the data of fusion reactions [13–16]. Many researchers have investigated that the influences of the shape deformations of the interacting nuclei (projectile or target) and vibrational states are important in changing the fusion cross sections, especially in the regions below the barrier [17–20]. The comprehension of the role of surface vibrational and rotational coupling effect of nuclei in the fusion reaction has been partially obtained, though many zones in this field are waiting to be discovered [21–25]. Since many properties of fusion reactions are not yet fully understood, it is a substantial working field to investigate the effects of different interaction combinations and excitations of nucleons and the effects of the nuclear structure of interacting couples on theoretical and experimental bases [26–29].

The methodical investigations involving mostly joint projectile (or target) are more enlightening than the singular state. In general, fusion reaction combinations, in which one of the interacting nuclei is stable, procure a preferable setting in the comprehension of the fusion parameters in the nearby of the Coulomb barrier. Under these circumstances, many researchers carried out their precursor investigation. Similar to our work,

empirical and theoretical studies have been conducted on the fusion reaction involving the bombardment of a stable ^{28}Si projectile over a series of stable Zr targets from stable nuclei with a small number of neutrons ^{90}Zr to stable nuclei with a large number of neutrons ^{96}Zr [30–35]. When the ascent of neutron abundance in the target nuclei, the ability of the rotation and vibration properties of the nuclei almost rises, and the relevant excitation energy decreases, *i.e.* the effects of different combinations of interactions (rotational and vibrational) on the fusion reaction are anticipated to rise with the increment of the number of neutrons in the target [35].

For ^{28}Si + ^{92}Zr, Newton *et al.* focused on the heavy ions (a beam of ^{28}Si in the energy interval E_{lab} of 86–107 MeV with 1 MeV energy steps on a ^{92}Zr target) accelerated by the ANU 14UD Pelletron accelerator in Australia which were pulsed to provide ≈ 1 ns extensive beam burst every 530 ns. Then they exactly gauged the fusion reaction data. Furthermore, they used the Coupled Channel model (via CCMOD code) to analyze the experimental data [30]. ^{28}Si + ^{90,94}Zr, Kalkal *et al.* focused on the heavy ions (a beam of ^{28}Si in the energy interval E_{lab} of 82–120 MeV with 2 MeV energy steps on a ^{90,94}Zr target) accelerated by the 15UD Pelletron accelerator at the Inter University Accelerator Centre (IUAC) in New Delhi, India, and then they exactly gauged the fusion reaction data. Next, they used the Coupled Channel model (via CCFULL code) to analyze the experimental data [31]. For ^{28}Si + ^{92,96}Zr, Khushboo *et al.* focused on the heavy ions (a beam of ^{28}Si in the energy interval E_{lab} of 81.4–119.5 MeV on a ^{92,96}Zr target) accelerated by the Pelletron accelerator of Inter University Accelerator Centre (IUAC), in New Delhi, India, and they used the Coupled Channel model (via CCFULL code) to analyze the experimental data. Gautam *et al.* using these experimental results, worked theoretically to search the effect of neutron transfer channels and/or collective inelastic surface excitations in the fusion of ^{28}Si with ^{90,92,94,96}Zr targets via the Coupled Channel (CC) and the Energy-dependent Woods–Saxon potential (EDWSP) models [35].

With the motivation we got from the studies briefly mentioned above, we wanted to theoretically examine the data of the ^{30}Si + ^{90,92,94,96}Zr reactions, which were not included in the literature in these works, and published them. We detailed interrogated the effects of phonon number in the projectile and target nuclei on heavy-ion fusion cross sections and barrier distributions. These computations were executed with the handling of the NRV [36–39], CCFULL [6, 15], and Wong's formula [40, 41]. Data are investigated theoretically through EDWSP and CC models which are described in Section 2. The results and discussions section implicates the outputs of our computations. In the final section, we abridged our outputs and presented our conclusions.

2. Fusion cross section and barrier distributions formalism

2.1. Energy-dependent Woods–Saxon Potential (EDWSP) model

We can define the total fusion cross section via the partial wave solution as

$$\sigma_{\mathrm{F}} = \frac{\pi}{k^2}\sum_{l=0}^{\infty}(2l+1)T_l^{\mathrm{F}}\,, \tag{1}$$

where μ is the reduced mass of interacting nucleus and E_{cm} is the energy in the center-of-mass frame. Barrier penetration probability T_l^{F} for the Hill–Wheeler formula is a function [42]

$$T_l^{\mathrm{HW}} = \frac{1}{1+\exp\left[(2\pi/\hbar w_l)\,(V_l - E_{\mathrm{cm}})\right]}\,, \tag{2}$$

where V_l is the barrier height and $\hbar_{wl}$ is the barrier curvature of l^{th} partial wave. We write this expression within Eq. (1),

$$\sigma_{\mathrm{F}} = \frac{\pi}{k^2}\sum_{l=0}^{\infty}(2l+1)\frac{1}{1+\exp\left[(2\pi/\hbar w_l)\,(V_l - E_{\mathrm{cm}})\right]}\,. \tag{3}$$

This statement has been rearranged to make it clearer by Wong [40]

$$R_l = R_{l=0} = R_{\mathrm{B}}\,, \tag{4}$$

$$\omega_l = \omega_{l=0} = \omega\,, \tag{5}$$

$$V_l = V_{\mathrm{B0}} + \frac{\hbar^2}{2\mu {R_{\mathrm{B}}}^2}\left[l+\frac{1}{2}\right]^2\,, \tag{6}$$

where, V_{B0} is the barrier height and R_{B} is the barrier position (radius). With the help of these expressions, we rewrite the formula known as Wong's formula for cross sections [40]

$$\sigma_{\mathrm{F}} = \frac{\hbar w}{2E_{\mathrm{cm}}}R_{\mathrm{B}}^2\ln\left[1+\exp\left(\frac{2\pi}{\hbar w}\,(2E_{\mathrm{cm}} - V_{\mathrm{B0}})\right)\right]\,. \tag{7}$$

Here, it can be viewed that the cross section is computed with the help of three coefficients: the barrier curvature $\hbar w$, the barrier radius R_{B}, and the barrier height V_{B0}, whereas around the Coulomb barrier it would look as follows:

$$\sigma_{\mathrm{F}} = \pi {R_{\mathrm{B}}}^2\left[1-\frac{V_{\mathrm{B0}}}{E_{\mathrm{cm}}}\right]\,; \qquad E_{\mathrm{cm}} > V_{\mathrm{B0}}\,, \tag{8}$$

$$\sigma_{\mathrm{F}} \approx {R_{\mathrm{B}}}^2\frac{\hbar w}{2E_{\mathrm{cm}}}\exp\left(\frac{2\pi}{\hbar w}\,(2E_{\mathrm{cm}} - V_{\mathrm{B0}})\right)\,; \qquad E_{\mathrm{cm}} < V_{\mathrm{B0}}\,. \tag{9}$$

For Wong's barrier distributions, the following equation is used [40, 41]:

$$\frac{\mathrm{d}^2(E\sigma_{\mathrm{F}})}{\mathrm{d}E^2} = \pi {R_{\mathrm{B}}}^2 \frac{2\pi}{\hbar w}\left(\frac{\mathrm{e}^x}{1+\mathrm{e}^x}\right)^2 ; \qquad x = \frac{2\pi}{\hbar w}(E_{\mathrm{cm}} - V_{\mathrm{B0}})\,. \tag{10}$$

In the EDWSP model, the nuclear potential is approved to be of the Woods–Saxon model, which is described as

$$V_N(r) = \frac{-V_0}{1} + \exp\left[\frac{(r-R_0)}{a_0}\right] ; \qquad R_0 = r_0\left[A_{\mathrm{P}}^{1/3} + A_{\mathrm{T}}^{1/3}\right] , \tag{11}$$

where V_0 is the depth coefficient, a is the position coefficient, A_{P} and A_{T} are the mass number of projectile and target nuclei. The Coulomb potential among interacting nuclei is characterized as

$$V_{\mathrm{C}}(r) = \frac{Z_{\mathrm{P}} Z_{\mathrm{T}} e^2}{r} , \tag{12}$$

where Z_{P} and Z_{T} terms denote the charge of the projectile and the target nuclei. For the EDWSP model, the depth coefficient is characterized as

$$\begin{aligned} V_0 \;=\; & \left[A_{\mathrm{P}}^{1/3} + A_{\mathrm{T}}^{1/3} - (A_{\mathrm{P}} + A_{\mathrm{T}})^{1/3}\right] \\ & \times \left[2.38 + 6.8(1 + I_{\mathrm{P}} + I_{\mathrm{T}})\frac{A_{\mathrm{P}}^{1/3} A_{\mathrm{T}}^{1/3}}{A_{\mathrm{P}}^{1/3} + A_{\mathrm{T}}^{1/3}}\right] \ \mathrm{MeV}\,, \end{aligned} \tag{13}$$

where A_{P} and A_{T} are the mass number of the projectile and target nuclei. The isospin asymmetry dynamics for projectile and target nuclei can be defined as

$$I_{\mathrm{P}} = \left(\frac{N_{\mathrm{P}} - Z_{\mathrm{P}}}{A_{\mathrm{P}}}\right) ; \qquad I_{\mathrm{T}} = \left(\frac{N_{\mathrm{T}} - Z_{\mathrm{T}}}{A_{\mathrm{T}}}\right) . \tag{14}$$

This model limits the potential depth for the system where the charge of the projectile and target nuclei combination is from $Z_{\mathrm{P}} Z_{\mathrm{T}} = 84$ to $Z_{\mathrm{P}} Z_{\mathrm{T}} = 1640$. Static and dynamic effects of fusion reactions generally take place in the surface of the nuclear potential or the tail area of the Coulomb barrier. All these mentioned impacts provide the change of potential coefficients. Surface impacts, namely coupled channel impacts, provide an increase in fusion in the energies under the barrier.

Finally, we can define the position parameter for the EDWSP model as

$$a(E) = 0.85\left[1 + \frac{r_0}{13.75\left(A_{\mathrm{P}}^{-1/3} + A_{\mathrm{T}}^{-1/3}\right)\left[1 + \exp\left(\frac{\frac{E}{V_{\mathrm{B0}}} - 0.96}{0.03}\right)\right]}\right] \ \mathrm{fm}\,. \tag{15}$$

2.2. Coupled Channel (CC) model

In this section, we presented the CC model for the heavy-ion fusion reaction systems. The undermentioned series of coupled channel equations are to be decoded statistically via this model [6, 8, 43–45]

$$\left[-\frac{\hbar^2}{2\mu}\frac{\mathrm{d}^2}{\mathrm{d}r^2}+\frac{J(J+1)\hbar^2}{2\mu r^2}+V_N^0(r)+\frac{Z_{\mathrm{P}}Z_{\mathrm{T}}e^2}{r}+\varepsilon_n-E\right]$$
$$\times\psi_n(r)+\sum_m V_{nm}(r)\psi_m(r)=0\,. \tag{16}$$

In this equation, respectively, μ, E_{cm}, and ε_n refer to the reduced mass of the projectile–target nuclei, the energy in the center-of-mass frame, and the excitation energy of the n^{th} channel. While V_{nm} symbolizes the matrix components of the Hamiltonian consisting of Coulomb and nuclear terms, the term r is the radial coordinate between interacting nuclei. When the degrees of freedom are included, the fusion cross section is expressed as

$$\sigma_{\mathrm{F}}(E_{\mathrm{cm}})=\sum_j \sigma_j E_{\mathrm{cm}}=\frac{\pi}{k_0^2}\sum_j(2j+1)P_J(E_{\mathrm{cm}})\,. \tag{17}$$

The term $P_J(E_{\mathrm{cm}})$ seen in this equation is expressed as the transmission parameter related to the angular momentum J. The Hamiltonian processors for rotational (deformed) and vibrational coupled channels are expressed as

$$\hat{O}_{\mathrm{R}} = \beta_2 R_{\mathrm{T}} Y_{20}+\beta_4 R_{\mathrm{T}} Y_{40}\,, \tag{18}$$
$$\hat{O}_{\mathrm{V}} = \frac{\beta_\lambda}{\sqrt{4\pi}} R_{\mathrm{T}}\left(a^\dagger_{\lambda 0}+a_{\lambda 0}\right)\,, \tag{19}$$

where, $R_{\mathrm{T}}=r_0(A_p^{1/3})$, β_λ and $(a^\dagger_{\lambda 0}+a_{\lambda 0})$ implie the deformation parameters and the derivation (extinction) processor of the phonon of the vibrational state of multipolarities λ. The nuclear coupling matrix components are defined as

$$V^{\mathrm{N}}_{nm}=\left\langle n\left|V_{\mathrm{N}}\left(r,\hat{O}\right)\right|\right\rangle - V^{(0)}_{\mathrm{N}}\delta_n,m\,. \tag{20}$$

For rotational and vibrational coupled states, the matrix components are expressed as

$$\hat{O}_{\mathrm{R}(I,I')} = \sqrt{\frac{5(2I+1)\,(2I'+1)}{4\pi}}\beta_2 R_{\mathrm{T}}\begin{pmatrix} I & 2 & I' \\ 0 & 0 & 0\end{pmatrix}^2$$
$$+\sqrt{\frac{9(2I+1)\,(2I'+1)}{4\pi}}\beta_4 R_{\mathrm{T}}\begin{pmatrix} I & 4 & I' \\ 0 & 0 & 0\end{pmatrix}^2\,, \tag{21}$$
$$\hat{O}_{\mathrm{V}(n,m)} = \frac{\beta_\lambda}{\sqrt{4\pi}} R_{\mathrm{T}}\left(\delta_{n,m-1}\sqrt{m}+\delta_{n,m+1}\sqrt{n}\right)\,. \tag{22}$$

The matrix components are calculated via the linear coupling approach and illustrated as

$$V^{(\mathrm{C})}_{\mathrm{V}(n,m)} = \frac{\beta_\lambda}{\sqrt{4\pi}} \frac{3}{2\lambda+1} Z_\mathrm{P} Z_\mathrm{T} e^2 \frac{R^\lambda_\mathrm{T}}{r^\lambda} \left(\sqrt{m}\, \delta_{n,m-1} + \sqrt{n}\, \delta_{n,m+1} \right) , \tag{23}$$

$$V^{(\mathrm{C})}_{\mathrm{R}(I,I')} = \frac{3 Z_\mathrm{P} Z_\mathrm{T}}{R^2_\mathrm{T}} 5r^3 \sqrt{\frac{5(2I+1)\,(2I'+1)}{4\pi}} \left(\beta_2 + \frac{2}{7}\beta_2^2 \sqrt{\frac{5}{\pi}} \right) \begin{pmatrix} I & 2 & I' \\ 0 & 0 & 0 \end{pmatrix}^2$$
$$+ \frac{3 Z_\mathrm{P} Z_\mathrm{T} R^4_\mathrm{T}}{9r^5} \sqrt{\frac{9(2I+1)\,(2I'+1)}{4\pi}} \left(\beta_4 + \frac{9}{7}\beta_2^2 \sqrt{\frac{5}{\pi}} \right) \begin{pmatrix} I & 4 & I' \\ 0 & 0 & 0 \end{pmatrix}^2 . \tag{24}$$

The total coupling matrix components are achieved via accumulation of $V^{(\mathrm{N})}_{nm}$ and $V^{(\mathrm{C})}_{nm}$.

3. Results and discussions

In this chapter, we offer our theoretical investigation outcomes via the EDWSP and CC models for the ^{30}Si + ^{90,92,94,96}Zr reaction series.

All calculus was executed with the handling of the NRV [36–39], CCFULL [6, 15], and Wong's formula [40, 41] through EDWSP and CC models. In this work, it should be especially emphasized that ^{30}Si, ^{94}Zr, and ^{96}Zr nuclei are deformed and have to be treated as rotators, besides this, ^{90}Zr and ^{92}Zr nuclei are treated as having the vibrational intrinsic spectra (as can be seen in Fig. 1).

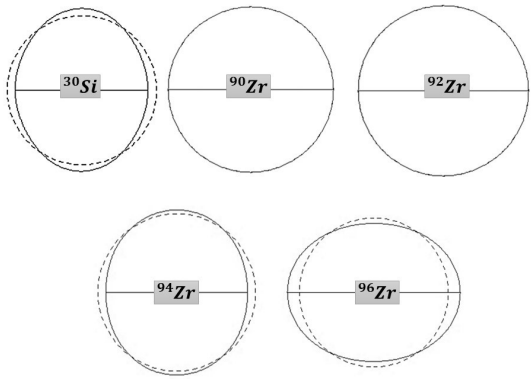

Fig. 1. The shapes of the interacting nuclei according to their deformation parameters.

The rotational (deformed) states of the ^{30}Si nucleus has the following deformation parameters [46–49]: $E_{2^+} = 2.2353$ MeV, $\beta_2 = -0.236$ and $\beta_4 = 0.040$. In like manner, the rotational (deformed) states for the ^{94}Zr

nucleus have the ensuing parameters [46–49]: $E_{2^+} = 0.9188$ MeV, $\beta_2 = -0.156$, $\beta_4 = -0.003$ and for the ^{96}Zr nucleus have the ensuing parameters [46–49]: $E_{2^+} = 1.7505$ MeV, $\beta_2 = 0.240$, $\beta_4 = 0.011$. In addition, these vibrational states for the ^{90}Zr nucleus have the ensuing parameters [46–49]: $E_{2^+} = 2.1863$ MeV, $\beta_{2^+} = 0.0907$, $E_{3^-} = 2.748$ MeV, $\beta_{3^-} = 0.211$, and for the ^{92}Zr nucleus [46–49]: $E_{2^+} = 0.9345$ MeV, $\beta_{2^+} = 0.100$, $E_{3^-} = 2.340$ MeV, $\beta_{3^-} = 0.174$. Taking into consideration these characteristics of the projectile and target nuclei, we obtain fairly good agreement between theoretical predictions for the fusion cross section and barrier distribution functions.

We have analyzed respectively the $^{30}\mathrm{Si} + ^{90,92,94,96}\mathrm{Zr}$ reaction series cross sections and barrier distributions at 2.0 MeV paces in the energy interval of 60–96 MeV. The multiples of the nuclear potential were assigned for each reaction and demonstrated in Table 1. Moreover, we received the integration coefficients as $R_{\max} = 25$ fm and integration paces $h = 0.05$ fm in calculations.

Table 1. The barrier peculiarities such as V_{B0}, R_{B}, and $\hbar\omega$ as handled in the EDWSP and CC models computations of fusion cross section and barrier distributions for our $^{30}\mathrm{Si} + ^{90,92,94,96}\mathrm{Zr}$ reaction series.

Reaction	V_{B0} [MeV]	R_{B} [fm]	$\hbar\omega$ [MeV]	Ref.
$^{30}\mathrm{Si} + ^{90}\mathrm{Zr}$	70.02	10.52	3.31	[6]
$^{30}\mathrm{Si} + ^{92}\mathrm{Zr}$	69.61	10.59	3.30	[6]
$^{30}\mathrm{Si} + ^{94}\mathrm{Zr}$	69.22	10.66	3.28	[6]
$^{30}\mathrm{Si} + ^{96}\mathrm{Zr}$	69.85	10.72	3.27	[6]

The Woods–Saxon (WS) and EDWSP parameter values are inscribed in Tables 2 and 3 for the same reactions, respectively.

Table 2. Height, potential, and position parameters of WS potential handled in the CC calculations for our $^{30}\mathrm{Si} + ^{90,92,94,96}\mathrm{Zr}$ reaction series.

Reaction	r_0 [fm]	V_0 [MeV]	a [MeV]	Refs.
$^{30}\mathrm{Si} + ^{90}\mathrm{Zr}$	1.176	67.347	0.663	[50–53]
$^{30}\mathrm{Si} + ^{92}\mathrm{Zr}$	1.176	67.437	0.664	[50–53]
$^{30}\mathrm{Si} + ^{94}\mathrm{Zr}$	1.176	67.528	0.664	[50–53]
$^{30}\mathrm{Si} + ^{96}\mathrm{Zr}$	1.177	67.619	0.664	[50–53]

Table 3. Height, potential, and position parameters of WS potential handled in the CC calculations for our ^{30}Si + ^{90,92,94,96}Zr reaction series.

Reaction	r_0 [fm]	V_0 [MeV]	$\frac{a^{\text{present}}}{\text{energy range}}$ $[\frac{\text{fm}}{\text{MeV}}]$	Ref.
^{30}Si + ^{90}Zr	1.100	92.365	$\frac{0.97-0.85}{60 \text{ to } 90}$	[35]
^{30}Si + ^{92}Zr	1.100	94.378	$\frac{0.97-0.85}{60 \text{ to } 90}$	[35]
^{30}Si + ^{94}Zr	1.100	96.340	$\frac{0.97-0.85}{60 \text{ to } 90}$	[35]
^{30}Si + ^{96}Zr	1.100	98.253	$\frac{0.97-0.85}{60 \text{ to } 90}$	[35]

All calculation results are exhibited in Fig. 2 to Fig. 7, which demonstrate fusion cross sections and barrier distributions for the ^{30}Si+^{90,92,94,96}Zr reaction series respectively. As can be seen from all figures, handled computation models, codes, and parameters are in fine connection with each other. In spite of there being a little few disagreements in the areas below the barrier region, computations mostly realized a good coherence foregoing the barrier area for cross sections.

In Fig. 2, the ^{30}Si + ^{90}Zr reaction, cross-section outputs alter from 1.007×10^{-8} mb to 853.4 mb and the barrier distributions outputs alter from 1.620 mb/MeV to 421.900 mb/MeV for no-excitations computations at 2.0 MeV steps in the energy interval of 60–96 MeV. For the rotational projectile nuclei and 2^+ vibrational target nuclei calculations, outputs alter from 1.344×10^{-9} mb to 753.300 mb via NRV and from 1.471×10^{-7} mb to 832.300 mb via CCFULL. The barrier distributions outputs alter from -5.962 mb/MeV to -14.640 mb/MeV for the rotational projectile nuclei and

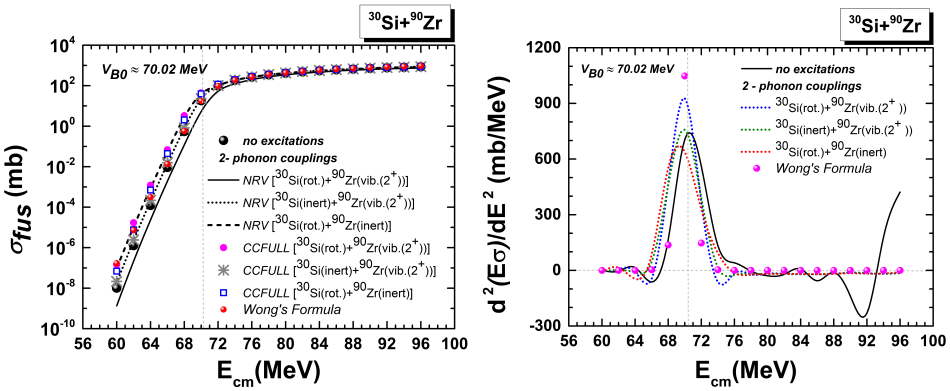

Fig. 2. The fusion cross sections and barrier distribution functions for the ^{30}Si+^{90}Zr reaction through EDWSP and CC models with the quadrupole 2^+ vibrational combinations of the target nucleus.

2^+ vibrational target nuclei calculations. For the inert projectile nuclei and 2^+ vibrational target nuclei calculations, outputs alter from 1.848×10^{-8} mb to 858.600 mb via NRV and from 2.158×10^{-8} mb to 866.900 mb via CCFULL. The barrier distributions outputs alter from -5.962 mb/MeV to -14.640 mb/MeV for the inert projectile nuclei and 2^+ vibrational target nuclei calculations. For the rotational projectile nuclei and inert target nuclei calculations, outputs alter from 9.653×10^{-8} mb to 861.800 mb via NRV and from 6.941×10^{-8} mb to 882.100 mb via CCFULL. Wong's formula cross-section outputs alter from 1.692×10^{-7} mb to 940.400 mb. The barrier distributions outputs alter from -8.587 mb/MeV to -11.370 mb/MeV for the rotational projectile nuclei and inert target nuclei calculations. Wong's formula barrier distributions calculations change from 3.654 mb/MeV to 2.583 mb/MeV.

In Fig. 3, for the $^{30}\mathrm{Si} + {}^{90}\mathrm{Zr}$ reaction, cross-section outputs alter from 9.997×10^{-9} mb to 763.100 mb and the barrier distributions outputs alter from 1.830 mb/MeV to 442.500 mb/MeV for no-excitations computations at 2.0 MeV steps in the energy interval of 60–96 MeV. For the rotational projectile nuclei and 3^- vibrational target nuclei calculations, outputs alter from 1.424×10^{-7} mb to 894.900 mb via NRV and from 2.921×10^{-7} mb to 850.300 mb via CCFULL. The barrier distributions outputs alter from -4.132 mb/MeV to 438.400 mb/MeV for the rotational projectile nuclei and 3^- vibrational target nuclei calculations. For the inert projectile nuclei and 3^- vibrational target nuclei calculations, outputs alter from 1.918×10^{-8} mb to 868.600 mb via NRV and from 2.158×10^{-8} mb to 875.900 mb via CCFULL. The barrier distributions outputs alter from -8.816 mb/MeV to -18.620 mb/MeV for the inert projectile nuclei and 3^- vibrational target

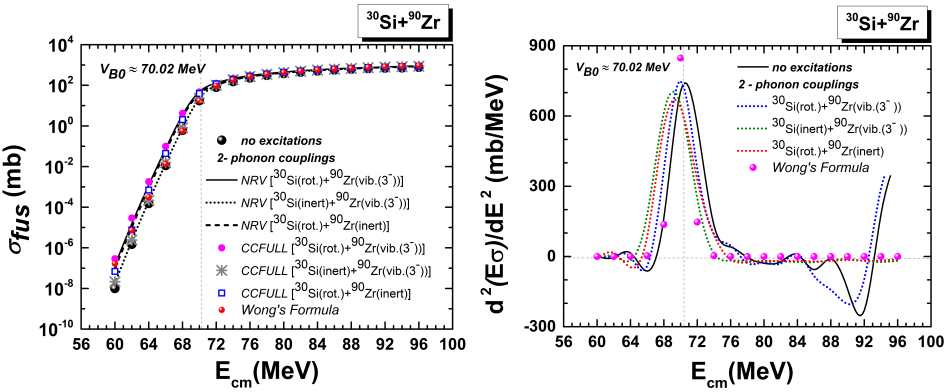

Fig. 3. The fusion cross sections and barrier distribution functions for the $^{30}\mathrm{Si} + {}^{90}\mathrm{Zr}$ reaction through EDWSP and CC models with the octupole 3^- vibrational combinations of the target nucleus.

nuclei calculations. For the rotational projectile nuclei and inert target nuclei calculations, outputs alter from 9.653×10^{-8} mb to 861.800 mb via NRV and from 6.941×10^{-8} mb to 882.100 mb via CCFULL. Wong's formula cross-section outputs alter from 1.692×10^{-7} mb to 940.400 mb. The barrier distributions outputs alter from −8.677 mb/MeV to −11.760 mb/MeV for the rotational projectile nuclei and inert target nuclei calculations. Wong's formula barrier distribution outputs alter from 3.795 mb/MeV to 2.792 mb/MeV.

In the no-coupled excitations specification, the projectile nuclei and target nuclei are taken as inert. It is clear from Figs. 2 and 3 that the effect of octupole vibrational states of the target nucleus on coupled channel calculations is greater than that of quadrupole vibrational states, namely the 3^- vibrational state can be expressed to be more effective than the 2^+ one.

It is monitored that the CC and phonon excitation impressions increased the calculated cross sections around the Coulomb barrier energies. As can be seen in Figs. 2 and 3, in spite of very small disagreements below the barrier area, all fusion cross-section outputs usually achieved a fine coherence afore the barrier area. The handled models, codes, and parameters are in fine coherence with each other.

It is substantial for the fusion dynamics of the reaction that the target nucleus has a spherical (vibrational) shape in the ground state, and the projectile has a deformed flat shape in the ground state. Since the excitation energy of the quadrupole vibrational state of the target is lesser than that of octupole vibrations, this situation is understandably reflected in our theoretical calculation results presented in Figs. 4 and 5. In Fig. 4, for the $^{30}\mathrm{Si}+{}^{92}\mathrm{Zr}$ reaction, cross-section outputs alter from 2.467×10^{-8} mb to 878.500 mb and the barrier distributions outputs alter from −8.831 mb/MeV to −14.450 mb/MeV for no-excitations calculations at 2.0 MeV paces in the

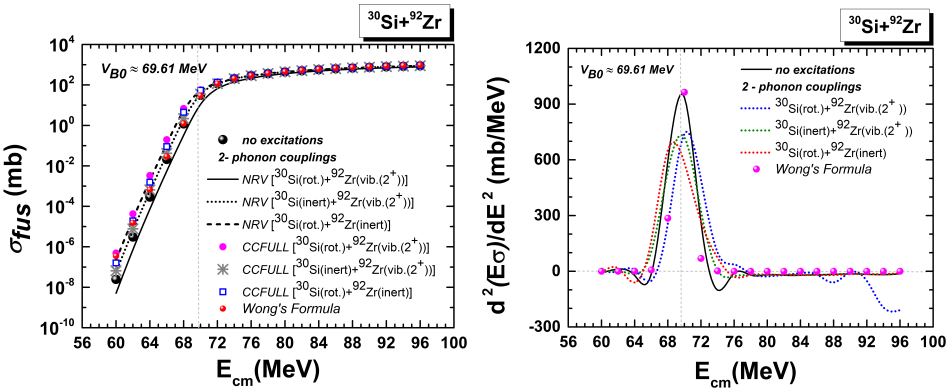

Fig. 4. The fusion cross sections and barrier distribution functions for the $^{30}\mathrm{Si}+{}^{92}\mathrm{Zr}$ reaction through EDWSP and CC models with the quadrupole 2^+ vibrational combinations of the target nucleus.

energy interval of 60–96 MeV. For the rotational projectile nuclei and 2^+ vibrational target nuclei calculations, outputs alter from 5.118×10^{-9} mb to 779.100 mb via NRV and from 4.903×10^{-7} mb to 879.100 mb via CCFULL. The barrier distribution outputs alter from -1.077 mb/MeV to -209.300 mb/MeV for the rotational projectile nuclei and 2^+ vibrational target nuclei calculations. For the inert projectile nuclei and 2^+ vibrational target nuclei calculations, outputs alter from 5.592×10^{-8} mb to 879.600 mb via NRV and from 6.533×10^{-8} mb to 896.100 mb via CCFULL. The barrier distribution outputs alter from -8.274 mb/MeV to -11.390 mb/MeV for the inert projectile nuclei and 2^+ vibrational target nuclei calculations. For the rotational projectile nuclei and inert target nuclei calculations, outputs alter from 2.242×10^{-7} mb to 886.900 mb via NRV and from 1.605×10^{-7} mb to 911.800 mb via CCFULL. Wong's formula cross-sections outputs alter from 3.521×10^{-7} mb to 968.000 mb. The barrier distribution outputs alter from -6.679 mb/MeV to -10.940 mb/MeV for the rotational projectile nuclei and inert target nuclei calculations. Wong's formula barrier distribution outputs alter from 6.945 mb/MeV to 1.036×10^{-18} mb/MeV.

In Fig. 5, for the $^{30}\mathrm{Si} + {}^{92}\mathrm{Zr}$ reaction, cross-section outputs alter from 2.527×10^{-8} mb to 881.500 mb and the barrier distribution outputs alter from -8.923 mb/MeV to -15.730 mb/MeV for no-excitations calculations at 2.0 MeV paces in the energy interval of 60–96 MeV. For the rotational projectile nuclei and 3^- vibrational target nuclei calculations, outputs alter from 1.505×10^{-8} mb to 778.600 mb via NRV and from 1.673×10^{-6} mb to 881.600 mb via CCFULL. The barrier distribution outputs alter from -5.88 mb/MeV to -548.400 mb/MeV for the rotational projectile nuclei and 3^- vibrational target nuclei calculations. For the inert projectile nuclei and 3^- vibrational target nuclei calculations, outputs alter from 1.769×10^{-7} mb to 906.800 mb via NRV and from 3.122×10^{-7} mb to 883.500 mb via

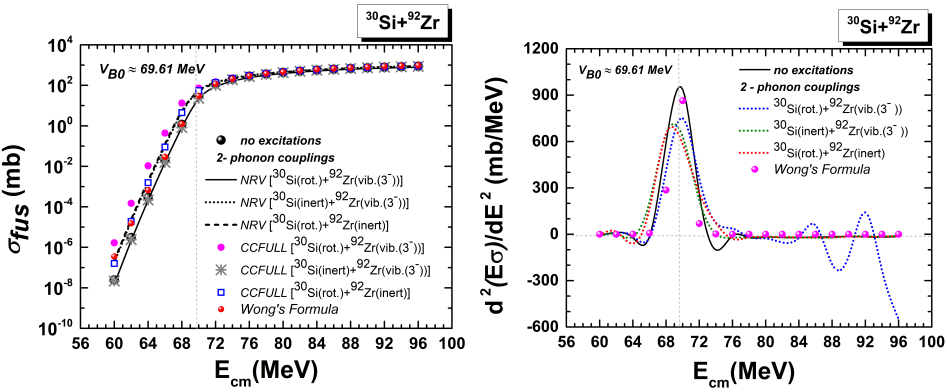

Fig. 5. The fusion cross sections and barrier distribution functions for the $^{30}\mathrm{Si} + {}^{92}\mathrm{Zr}$ reaction through EDWSP and CC models with the octupole 3^- vibrational combinations of the target nucleus.

CCFULL. The barrier distribution outputs alter from −8.009 mb/MeV to −10.680 mb/MeV for the inert projectile nuclei and 3^- vibrational target nuclei calculations. For the rotational projectile nuclei and inert target nuclei calculations, outputs alter from 2.322×10^{-7} mb to 892.500 mb via NRV and from 1.711×10^{-7} mb to 923.400 mb via CCFULL. Wong's formula cross-sections outputs alter from 3.521×10^{-7} mb to 968.000 mb. The barrier distribution outputs alter from −6.679 mb/MeV to −10.940 mb/MeV for the rotational projectile nuclei and inert target nuclei calculations. Wong's formula barrier distribution outputs alter from 7.651×10^{-5} mb/MeV to 1.042×10^{-18} mb/MeV.

In the no-coupled excitations specification, the projectile and target are taken as inert. It is clear from Figs. 4 and 5 that the effect of octupole vibrational states of the target nucleus on coupled channel calculations is greater than that of quadrupole vibrational states, namely the 3^- vibrational state can be expressed to be more effective than the 2^+ vibrational state. It is viewed that the CC and phonon excitation impacts increased the calculated fusion cross section around the Coulomb barrier area. As can be seen in Figs. 4 and 5, in spite of very small disagreements below the barrier area, all fusion cross-section outputs usually achieved a fine coherence afore the barrier area. The handled models, codes, and parameters are in fine coherence with each other. Additionally, for vibrational states and their alternate couplings of the target nucleus, these calculations may be little deflected from the general fusion data at below barrier energy regions as glaring from Figs. 2 to 5.

In Fig. 6, for the $^{30}Si + {}^{94}Zr$ reaction, cross-section outputs alter from 5.819×10^{-8} mb to 902.8 mb and the barrier distributions outputs alter from −9.939 mb/MeV to −17.7004 mb/MeV for no-excitations calculations at 2.0 MeV paces in the energy interval of 60–96 MeV. For the rotational projectile nuclei and target nuclei calculations, cross-section outputs alter from 1.618×10^{-6} mb to 923.800 mb. The barrier distributions outputs alter from 9.928 mb/MeV to −9.499 mb/MeV for the rotational projectile nuclei and target nuclei calculations. For the inert projectile nuclei and rotational target nuclei calculations, cross-section outputs alter from 5.011×10^{-7} mb to 911.400 mb. The barrier distributions outputs alter from −5.494 mb/MeV to −10.240 mb/MeV for the inert projectile nuclei and rotational target nuclei calculations. For the rotational projectile nuclei and inert target nuclei calculations, cross-section outputs alter from 2.2422×10^{-7} mb to 886.900 mb. Wong's formula cross-section outputs alter from 6.693×10^{-7} mb to 995.400 mb. The barrier distribution outputs alter from −0.817 mb/MeV to −8.791 mb/MeV for the rotational projectile nuclei and inert target nuclei calculations. Wong's formula barrier distributions outputs alter from 1.472×10^{-4} mb/MeV to 3.686×10^{-19} mb/MeV.

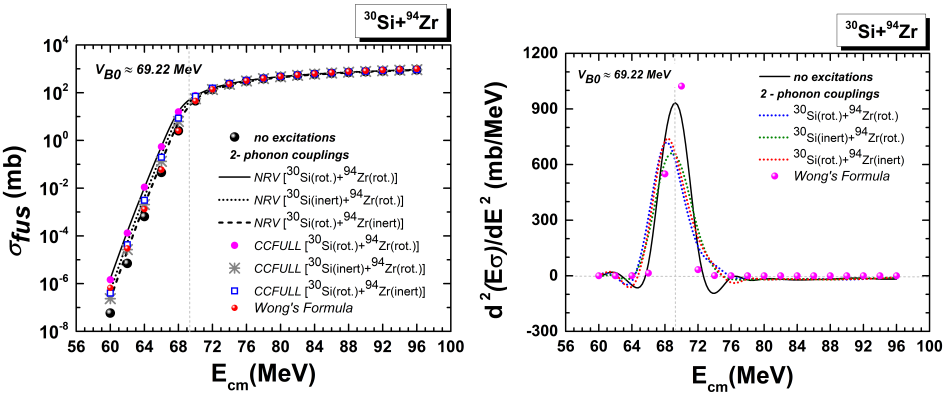

Fig. 6. The fusion cross sections and barrier distribution functions for the ^{30}Si + ^{94}Zr reaction through EDWSP and CC models with the rotational (deformed) combinations of the target nucleus.

When we compare the rotational (deformed) states containing two phonons with the no-excitations state for the ^{30}Si + ^{94}Zr reaction, it is seen in Fig. 6 that the cross section of the no-excitations state is lower. The barrier distributions soften when the phonons number alters and they start to alter mildly when phonons number is different from 0, they attain their smoothness at $n \approx 2$. In addition to this, the frame of barrier distributions sustains the same when a spacious number of phonons is considered in the coupled channel calculations.

As can be seen in Fig. 6, in spite of very small disagreements below the barrier area, all fusion cross-section outputs usually achieved a fine coherence afore the barrier area. The handled models, codes, and parameters are in fine coherence with each other.

For the ^{30}Si + ^{96}Zr reaction, the coupled channel computations about the no-excitations state are dramatically minor than that of the rotational (deformed) states containing two phonons as can be seen in Fig. 7. The impacts of rotational (deformed) states are quite large compared to the others.

In Fig. 7, for the ^{30}Si + ^{96}Zr reaction, cross-sections outputs alter from 1.336×10^{-7} mb to 926.600 mb and the barrier distribution outputs alter from -7.606 mb/MeV to -14.980 mb/MeV for no-excitations calculations at 2.0 MeV paces in the energy interval of 60–96 MeV. For the rotational projectile nuclei and target nuclei calculations, cross-section outputs alter from 5.990×10^{-5} mb to 950.000 mb. The barrier distributions outputs alter from 13.560 mb/MeV to -5.753 mb/MeV for the rotational projectile nuclei and target nuclei calculations. For the inert projectile nuclei and rotational target nuclei calculations, cross-section outputs alter from

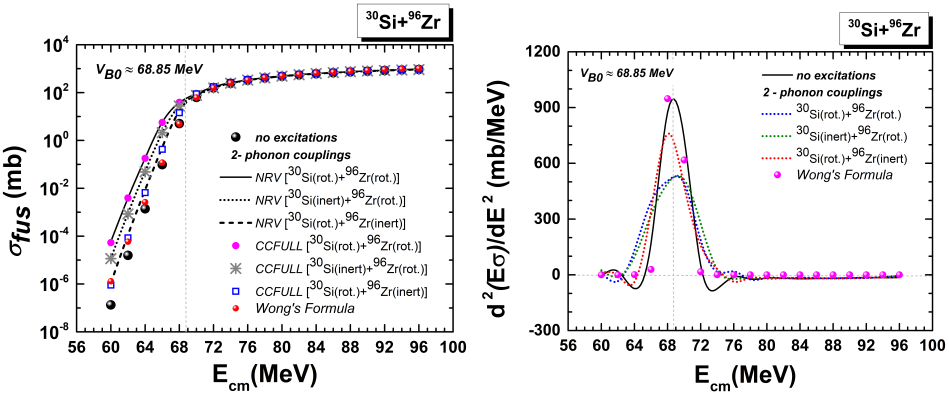

Fig. 7. The fusion cross sections and barrier distribution functions for the ^{30}Si + ^{96}Zr reaction through EDWSP and CC models with the rotational (deformed) combinations of the target nucleus.

1.197×10^{-5} mb to 932.900 mb. The barrier distributions outputs alter from 24.580 mb/MeV to −6.469 mb/MeV for the inert projectile nuclei and rotational target nuclei calculations. For the rotational projectile nuclei and inert target nuclei calculations, cross-section outputs alter from 1.103×10^{-6} mb to 935.500 mb. Wong's formula cross-section outputs alter from 1.301×10^{-6} mb to 1020.500 mb. The barrier distributions outputs alter from 10.340 mb/MeV to −13.780 mb/MeV for the rotational projectile nuclei and inert target nuclei calculations. Wong's formula barrier distributions outputs alter from 2.879×10^{-4} mb/MeV to 1.571×10^{-19} mb/MeV.

Consequently, the rotations in heavier targets (such as ^{94}Zr and^{96}Zr nuclei) are over intense and their impacts on the fusion duration of the consequential coaction may not be ignored and hereby is hoped to be a lot grander. To investigate some declinations between these forecasts and reaction, results are prominent for the refinement of heavy-ion researches infra barrier. Additionally, the efficacies of coupled channels on the fusion reaction are major and these efficacies are known to escalate as one acts from a stable target core with a minor number of neutrons (^{90}Zr) to a stable target core with a major number of neutrons (^{96}Zr).

Furthermore, we aimed to present to the reader the harmony or disharmony among calculation codes and methods. If experimental data are not available for the investigated fusion reactions, it is important to see how minor or major similarities and differences between methods affect the results using various techniques.

Mathematical (numerical) realizations are variant in some particulars, the alternative distinctions between the NRV and CCFULL; the NRV implements a more proper design for the matrix component reckoning, also

provides the chance to labor with the proximity potential, takes into account the nominal geometrical factor in the potential that is substantial when grand deformations play a part, and ensures a handy system [6, 36–39]. In other words, while NRV and CCFULL come in sight both in terms of entrance and output data, the major property that differentiates them from each other is the matrix component reckoning styles. The NRV code provides a new and advanced method for the numerical solution of CC equations [54, 55]. To come by a proper barrier distribution, fine and supereminence cross-sections knowledge is necessary, along with a handy quantitative technique to calculate the second derivative. Via this inspiration, we checked the barrier distributions acquired via NRV and CCFULL. The second derivative of Wong's formula is a theoretical computation formula that reproduces the empirical output. The calculations showed that Wong's formula reproduced the barrier distribution in an admissible technique confronted with theoretical calculations (NRV and CCFULL).

4. Conclusion

This theoretical investigation puts the emphasis on a way of understanding the principal effectiveness of the target–projectile couplings on the fusion interaction structure.

In our study, we have analyzed the ^{30}Si + ^{90,92,94,96}Zr fusion reaction series framework with different calculation codes and coupling configuration parameters at 2.0 MeV paces in the 60–96 MeV energy interval with various combinations of the projectile and target nuclei via EDWSP and CC models. All calculating outcomes are in exquisite compatibility with each other. NRV, CCFULL, and Wong's formula are handy and frequently modernized codes to achieve and strengthen dexterities and experimentation in adapting to advanced approximations to portray the qualifications of the nucleus and to be able to peruse the coefficients of reactions. In accordance with the starting plan of this study, the data obtained with the existing calculation methods gave handy and consistent results. Benchmarking the results of broad outputs relying on EDWSP and CC models with each other has expedited our explication of the effect of deformation coefficients and the importance of computation models on the reactions.

As a result of the calculations, it has been observed that spherical, that is, vibrating nuclei, and rotation, that is, deformed nucleus effects, are effective couplings that lead to large cross sections around the barrier. In the graphs, despite there being very small separations below the barrier region, cross-section computations mostly executed an explicit coherence with each other above the barrier zone. The computation procedure, codes, and coefficients are in fine coherence with each other. The EDWSP calculations reliably

predict cross sections and thus clearly explain cross sections around the barrier energies. The deformations (rotation effects) in heavier targets are more vigorous and their efficacies on the heavy-ion reactions of the relevant interaction may not be disregarded and, in consequence, are anticipated to be grander. To investigate some deflections between these predictions and sub-barrier, fusion results are major for the development of heavy-ion studies below barrier regions. In addition, the efficacies of the CC computations on the heavy-ion reactions are very substantial, and can be observed that such effects increase when comprehensive research is made from an isotope with few neutrons to isotopes with more neutrons.

In terms of guiding new research: more complex and different potentials can be used to further improve fusion calculations and investigations can be improved by handling different potentials and developing varied techniques for deformation coefficients. As a result, by arranging the coefficients most suitable for the experimental frameworks, we can make these datasets ready for future use as a preliminary in case the experimental conditions are not met.

REFERENCES

[1] Vijay *et al.*, «Fusion cross sections and barrier distributions for ^{16}O + ^{70,72,73,74}Ge and ^{18}O + ^{74}Ge reactions at energies near and below the Coulomb barrier», *Phys. Rev. C* **103**, 024607 (2021).

[2] A.M. Stefanini *et al.*, «New insights into sub-barrier fusion of ^{28}Si + ^{100}Mo», *J. Phys. G: Nucl. Part. Phys.* **48**, 055101 (2021).

[3] N.K. Deb *et al.*, «Role of neutron transfer in the sub-barrier fusion cross section in ^{18}O + ^{116}Sn», *Phys. Rev. C* **102**, 034603 (2020).

[4] R. Gharaei, H. Hasanzade, «Sub-barrier fusion of ^{34,36}Sn + ^{204,206,208}Pb: Signature of isotopic dependence of repulsive core potential in heavy-ion fusion reactions», *Nucl. Phys. A* **1013**, 122223 (2021).

[5] I.J. Thompson, «Coupled reaction channels calculations in nuclear physics», *Comput. Phys. Rep.* **7**, 167 (1988).

[6] K. Hagino, N. Rowley, A.T. Kruppa, «A program for coupled-channel calculations with all order couplings for heavy-ion fusion reactions», *Comput. Phys. Commun.* **123**, 143 (1999).

[7] M. Beckerman, «Sub-barrier fusion of two nuclei», *Rep. Prog. Phys.* **51**, 1047 (1988).

[8] V.I. Zagrebaev, «Heavy Ion Reactions at Low Energies», *Springer International Publishing*, Cham 2019, ISBN 978-3-030-27217-3.

[9] L.F. Canto, K. Hagino, M. Ueda, «Semi-classical approaches to heavy-ion reactions: fusion, rainbow, and glory», *Eur. Phys. J. A* **57**, 11 (2021).

[10] S.R. McGuinness *et al.*, «Production of ^{52}Fe from symmetric complete fusion-evaporation reactions», *Nucl. Instrum. Methods Phys. Res. B* **493**, 15 (2021).

[11] M. Rashdan, T.A. Abdel-Karim, «Microscopic description of the fusion excitation function of ^{32,36}S + ^{90,94,96}Zr», *Int. J. Mod. Phys. E* **29**, 2050046 (2020).

[12] A. Lépine-Szily, R. Lichtenthäler, «Coupled channels effects in heavy ion reactions», *Eur. Phys. J. A* **57**, 99 (2021).

[13] L.T. Baby *et al.*, «Role of ^{28}Si excitations in the sub-barrier fusion of ^{28}Si + ^{120}Sn», *Phys. Rev. C* **62**, 014603 (2000).

[14] A.M. Stefanini *et al.*, «Fusion of ^{40}Ca + ^{96}Zr revisited: Transfer couplings and hindrance far below the barrier», *Phys. Lett. B* **728**, 639 (2014).

[15] G. Colucci *et al.*, «Study of Sub-barrier Fusion of ^{36}S + ^{50}Ti, ^{51}V Systems», *Acta Phys. Pol. B* **51**, 769 (2020).

[16] M.S. Gautam, «Analysis of fusion dynamics of colliding systems involving stable, loosely bound and halo nuclei», *Phys. Scr.* **90**, 125301 (2015).

[17] M.S. Gautam, «Systematic failure of static nucleus–nucleus potential to explore sub-barrier fusion dynamics», *Phys. Scr.* **90**, 055301 (2015).

[18] W. Reisdorf, «Heavy-ion reactions close to the Coulomb barrier», *J. Phys. G: Nucl. Part. Phys.* **20**, 1297 (1994).

[19] B.B. Back, H. Esbensen, C.L. Jiang, K.E. Rehm, «Recent developments in heavy-ion fusion reactions», *Rev. Mod. Phys.* **86**, 317 (2014).

[20] M. Zamrun, Z.M.M. Mahmoud, N. Takigawa, K. Hagino, «Structure of ^{72,74}Ge nuclei probed with a combined analysis of heavy-ion fusion reactions and Coulomb excitation», *Phys. Rev. C* **81**, 044609 (2010).

[21] M.S. Gautam, K. Vinod, H. Kumar, «Role of Barrier Modification and Nuclear Structure Effects in Sub-Barrier Fusion Dynamics of Various Heavy Ion Fusion Reactions», *Braz. J. Phys.* **47**, 461 (2017).

[22] V. Tripathi *et al.*, «Isotopic dependence and channel coupling effects in the fusion of ^{16}O + ^{112,116}Sn and ^{32}S + ^{112,116,120}Sn at energies around the barrier», *Phys. Rev. C* **65**, 014614 (2001).

[23] V.Y. Denisov, «Subbarrier heavy ion fusion enhanced by nucleon transfer», *Eur. Phys. J. A* **7**, 87 (2000).

[24] V.V. Sargsyan *et al.*, «Effects of nuclear deformation and neutron transfer in capture processes, and fusion hindrance at deep sub-barrier energies», *Phys. Rev. C* **84**, 064614 (2011).

[25] V.N. Kodratyev, A. Bonasera, A. Iwamoto, «Kinetics in sub-barrier fusion of spherical nuclei», *Phys. Rev. C* **61**, 044613 (2000).

[26] B. Mei *et al.*, «Fusion reactions around the barrier for Be + ^{238}U», *Chinese Phys. C* **45**, 054001 (2021).

[27] A.A. Aziz, «Analysis of different proximity potentials applied to the ^{12}C + ^{12}C reaction», *AIP Conf. Proc.* **2319**, 040009 (2021).

[28] B.W. Asher *et al.*, «Experimental study of the $^{17}F + ^{12}C$ fusion reaction and its implications for fusion of proton-halo systems», *Phys. Rev. C* **103**, 044615 (2021).

[29] J. Mohammadi, O.N. Ghodsi, «Study of the dinuclear system for $^{296}119$ superheavy compound nucleus in fusion reactions», *Chinese Phys. C* **45**, 044107 (2021).

[30] J.O. Newton *et al.*, «Experimental barrier distributions for the fusion of ^{12}C, ^{16}O, ^{28}Si, and ^{35}Cl with ^{92}Zr and coupled-channels analyses», *Phys. Rev. C* **64**, 064608 (2001).

[31] S. Kalkal *et al.*, «Channel coupling effects on the fusion excitation functions for $^{28}Si + ^{90,94}Zr$ in sub- and near-barrier regions», *Phys. Rev. C* **81**, 044610 (2010).

[32] S. Kalkal *et al.*, «Multinucleon transfer reactions for the $^{28}Si + ^{90,94}Zr$ systems in the region below and near the Coulomb barrier», *Phys. Rev. C* **83**, 054607 (2011).

[33] S. Kalkal *et al.*, «Measurements and coupled reaction channels analysis of one- and two-proton transfer reactions for the $^{28}Si + ^{90,94}Zr$ systems», *Phys. Rev. C* **85**, 034606 (2012).

[34] Khushboo *et al.*, «Relationship between and effect of inelastic excitations and transfer channels on sub-barrier fusion enhancement», *Phys. Rev. C* **96**, 014614 (2017).

[35] M.S. Gautam *et al.*, «Influence of neutron transfer channels and collective excitations in the fusion of ^{28}Si with $^{90,92,94,96}Zr$ targets», *Phys. Rev. C* **102**, 014614 (2020).

[36] V.I. Zagrebaev, V.V. Samarin, «Near-barrier fusion of heavy nuclei: Coupling of channels», *Phys. Atom. Nuclei* **67**, 1462 (2004).

[37] NRV Web Knowledge Base on Low-Energy Nuclear Physics, `http://nrv.jinr.ru/nrv/`

[38] V.I. Zagrebaev, A. Kozhin, «Nuclear Reactions Video (knowledge base on low energy nuclear physics», JINR Report No. E10-99-151, 1999.

[39] A.S. Denikin *et al.*, «Modern Instruments for Nuclear Reaction Simulations Based on NRV Web Knowledge Base», *ALKU J. Sci. Spec. Issue* **NSP 2018**, 71 (2019).

[40] C.Y. Wong, «Interaction Barrier in Charged-Particle Nuclear Reactions», *Phys. Rev. Lett.* **31**, 766 (1973).

[41] J.M. Arias, M. Lozano, «An Advanced Course in Modern Nuclear Physics», *Springer Berlin Heidelberg*, Berlin, Heidelberg 2001, ISBN 978-3-540-44620-0.

[42] D.L. Hill, J.A. Wheeler, «Nuclear Constitution and the Interpretation of Fission Phenomena», *Phys. Rev.* **89**, 1102 (1953).

[43] K. Hagino, S. Kuyucak, N. Takigawa, «Excitation of nuclear anharmonic vibrations in heavy-ion fusion reactions», *Phys. Rev. C* **57**, 1349 (1998).

[44] K. Hagino *et al.*, «Importance of nonlinear couplings in fusion-barrier distributions and mean angular momenta», *J. Phys. G: Nucl. Part. Phys.* **23**, 1413 (1997).

[45] K. Hagino, T. Takehi, A.B. Balantekin, N. Takigawa, «Surface diffuseness anomaly in heavy-ion potentials for large-angle quasielastic scattering», *Phys. Rev. C* **71**, 044612 (2005).

[46] T. Kibedi, R.H. Spear, «Reduced Electric-Octupole Transition Probabilities, $B(E3; 0_1^+ \rightarrow 3_1^-)$ — An Update», *At. Data Nucl. Data Tables* **80**, 35 (2002).

[47] P. Möller, A.J. Sierk, T. Ichikawa, H. Sagawa, «Nuclear ground-state masses and deformations: FRDM(2012)», *At. Data Nucl. Data Tables* **109-110**, 1 (2016).

[48] B. Pritychenko, M. Birch, B. Singh, M. Horoi, «Tables of E2 transition probabilities from the first 2^+ states in even–even nuclei», *At. Data Nucl. Data Tables* **107**, 1 (2016).

[49] P. Raghavan, «Table of nuclear moments», *At. Data Nucl. Data Tables* **42**, 189 (1989).

[50] A. Winther, «Dissipation, polarization and fluctuation in grazing heavy-ion collisions and the boundary to the chaotic regime», *Nucl. Phys. A* **594**, 203 (1995).

[51] R.O. Akyuz, A. Winther, «Nuclear Structure and Heavy Ion Reactions», *North-Holland*, Amsterdam 1981.

[52] R.A. Broglia and A. Winther, «Heavy Ion Reactions, Part I and II, Frontiers in Physics», *Addison-Wesley*, 1991.

[53] A. Winther, «Grazing reactions in collisions between heavy nuclei», *Nucl. Phys. A* **572**, 191 (1994).

[54] Z.M. Cinan, B. Erol, T. Baskan, A.H. Yilmaz, «Heavy-Ion Fusion Reaction Calculations: Establishing the Theoretical Frameworks for ^{111}In Radionuclide over the Coupled Channel Model», *Energies* **14**, 8594 (2021).

[55] Z.M. Cinan, T. Baskan, B. Erol, A.H. Yilmaz, «Theoretical Inspecting of At-211 Radionuclide via Coupled-Channel Model for Fusion Reaction of Stable Nuclei», *Atom Indonesia* **47**, 163 (2021).